DECENTRALIZED FREQUENCY CONTROL OF POWER SYSTEMS WITH DEEP PENETRATION OF WIND-BASED GENERATION

BY

NABIL H. K. HIRZALLAH

THESIS

Submitted in partial fulfillment of the requirements
for the degree of Master of Science in Electrical and Computer Engineering
in the Graduate College of the
University of Illinois at Urbana-Champaign, 2015

Urbana, Illinois

Adviser:

Professor Petros G. Voulgaris

ABSTRACT

The introduction of the highly variable and uncertain renewable resources into the power grid is calling for more control and regulation of the power system dynamics. In particular, the automatic generation control, which is responsible for maintaining the nominal system frequency and the scheduled real power interchange, needs to be modified to include unmodeled system dynamics and to account for disturbances from renewable resources. In this thesis, we work on a nonlinear differential algebraic model of the power system which takes into account the effect of the power network and includes wind power injections. We then propose two decentralized controllers that each would stabilize the system frequency and power interchange. The first controller is based on linear quadratic (LQ) optimal control followed by an optimization algorithm to increase the sparsity of the feedback gains. The other controller is designed using the theory of overlapping control and the inclusion principle. Each controller is applied separately on a 3-machine 6-bus 2-wind turbine nonlinear model, and the simulation is carried out using Simulink. A power flow program is run at each automatic generation control (AGC) cycle to update the power flow variables. Results show that we can design decentralized controllers for each control area that can successfully track the desired frequency regardless of the disturbances associated with wind-based generation. Furthermore, we show that the performance of these controllers is comparable to that of a centralized controller.

ACKNOWLEDGMENTS

I would like to thank Professor Petros Voulgaris for his guidance and patience. I am grateful for the opportunity to be mentored and taught by him. I also would like to thank Abu Dhabi National Oil Company (ADNOC) for their support.

TABLE OF CONTENTS

CHAPTER 1

INTRODUCTION

1.1 Overview

Present schemes of automatic generation control (AGC) have evolved over the past 60 years and are implemented on very large interconnected systems across the US or in different parts of the world. However, the power grid has also been undergoing fast and major transformations in the last two decades seeking to become smarter, more efficient and cleaner [1]. Wind energy, in particular, gained growing importance around the world [2]. This renewable energy recorded the fastest growth rate among other renewable resources in the last few years [3]. It is anticipated to reach a worldwide production of 300 GW in 2015. The global penetration is predicted to reach 8% by 2020, whereas currently it is around 2.31% [3].

Due to the fact that wind energy cannot be stored and is considered to be non-dispatchable, i.e., the power output of each wind turbine cannot be determined beforehand, we are forced to treat the wind energy as uncontrollable, uncertain and highly variable [4]. These features make the wind turbines significantly different from conventional power generators. As the percentage of global penetration increases worldwide, there is a growing concern about the impacts on the power system operation and control. These concerns come from the fact that the variable property of wind energy and the uncertainties introduced in the system when operating a wind generator make it difficult to predict the performance of the system during abnormal power system operating conditions, and lead to challenges in developing mathematical frameworks that can simulate the behavior of the grid under high wind power penetration. As a result, wind farms might not be able to maintain acceptable levels of voltage and frequency across the power grid [5]. In fact, studies show that replacing conventional generators with wind tur-

bines decreases the overall inertia connected to the grid which causes faster frequency variations after abrupt variations in generation or load [6]. Recent studies have shown that heavy reliance on wind-based generation in the power system might cause overloading of transmission lines and overloading of tie-lines and fluctuation of system frequency and voltage in addition to negatively affecting optimum power flow, power quality and system security [7]. However, most published research on AGC systems neglects the impact of wind variability and uncertainty [8], [9], or suggests complex control structures that are usually impractical and difficult to implement. In addition, most present AGC systems employ simple and classical controllers that are tuned based on experience or trial and error, which may not be able to provide satisfactory dynamical performance over a wide range of operating conditions. As a result, large penetration of wind generators in the power grid calls for more regulation and poses important questions as to whether the traditional power system control in general, and frequency control in specific such as the AGC system, are still adequate to operate in the new environment.

The main objectives of any AGC system are to maintain the frequency of the grid and to maintain the power interchanges between neighboring areas at their scheduled values. This is achieved by controlling the units participating in AGC to follow the load profile and correct for errors in the load forecast. In this thesis, we want to extend AGC systems to include wind-based generation and the system network and try to meet the above objectives using modern control theory. The use of optimal control theory was first applied to the load frequency control (LFC) problem by Fosha and Elgerd in 1970 [10]. Their work focused on the application of linear quadratic state feedback controllers to the LFC problem. However, the controller they proposed lacked practicality since the amount of information required from the power system is significantly greater than what is required by the conventional control strategy. The controller not only needed measurements from the states of its own system, but also measurements form all connected systems. To solve this problem, sub-optimal controllers [11] and limited-state feedback controllers [12] were proposed over some performance loss.

1.2 Statement of Problem

In this thesis, we want to extend the AGC systems to include wind-based generation and the system network. However wind-based generation has unique features that make its impact on the system frequency different from conventional generators [13]. In regards to the network, it is believed that the network acts as a filter for the system with smoothing effects on the response of the closed-loop system [14]. In other words, the network lessens the effects of wind-based variability on the machine. Also the network can act as a physical constraint affecting the choice of machines compensating for wind-based generation variability. In the context of this thesis, the power injected by wind turbines can be described (under certain simplifying assumptions described in Section 2.1) as an uncertain disturbance to the system dynamics. Wind-based generation will be treated as negative load and subtracted from the actual system load. A power flow program is run at each AGC cycle to account for the network dynamics. We will use a three-state nonlinear machine model that includes the mechanical equations and the governor dynamics to simulate the system. For the time frame of interest for AGC, it is assumed that the disturbance introduced by the uncertain variations in wind-based generation around some nominal profile (given by forecast) is sufficiently small. Then, we linearize the mentioned DAE model along the nominal system trajectory, and by using Kron reduction, we reduce the resulting linear DAE model to an ordinary differential equation (ODE) model [14].

In an effort to design a decentralized controller, and to avoid relying on states that are not measured or transporting data over long distances between control areas, we use two methods to design two different decentralized controllers that each would stabilize the system. Then we compare the two controllers in terms of performance and sparsity of the controller gains (degree of decentralization).

For the first controller we use results from Lin et al. [15] to design an optimal sparse linear quadratic controller to adjust system frequency after load imbalances and to maintain the tie-line power between control areas. In their paper, Lin et al. design sparse feedback gains that minimize the $\mathcal{H}_2$ norm of distributed systems. They first identify a sparsity pattern of the feedback gains using sparsity-promoting penalty functions that penalize the

number of communication links in the distributed controller. Then, the authors attempt to solve an optimization problem of the state feedback gains subject to the structural sparsity constraints. Details of the optimization method will not be discussed in this thesis but the reader can refer to [15] for more information. The control action is applied on the machines participating in AGC only, while the wind turbines, although part of the system and generating power, will not be required to participate in the control action. The same control structure was applied in the power systems literature to stabilize inter-area oscillations between a group of generators which results from the dynamics of power transfers [16].

For the second controller we take advantage of the fact that we are stabilizing power systems that are formed by control areas where each control area defines a group of generators and loads that belong to one geographical area. As a result, the power system model can be treated as an interconnected system of overlapping subsystems. This allows us to consider overlapping control: as in [17], [18] and [19], it has been shown that systems composed of smaller overlapping subsystems can be expanded into a higher-dimensional space to separate the overlapping subsystems. Then, in the expanded space decentralized control laws for each subsystem can be designed and contracted back to the original space. For this thesis, we employ the theory of overlapping control to expand the power system model into subsystems that belong to the same control area, and then design a local controller for each area. The local controllers are then contracted back to the original space to obtain a decentralized controller for the whole system.

When compared to classical AGC results in the literature, the main novelty of the results presented in this thesis is the ability to design decentralized control laws that take into account the dynamics of the network (power flow) and reject the disturbances to the system frequency introduced by non-controllable wind-based generation. The application of the proposed AGC system is illustrated through a 3-machine, 6-bus system, which is a smaller version of the 3-machine, 9-bus model of the Western System Coordinating Council (WECC) system [20].

CHAPTER 2

MODELING FRAMEWORK

In this chapter, we present the modeling framework, which includes the wind-based electricity model, the power system DAE, and the linearized augmented model that results from accounting for the dynamics of wind-based electricity sources. This model is mainly derived using the work in [14].

2.1 Wind-Based Electricity Resource Model

Results from [21] and [22] show that a low-order dynamical model for a Type-C wind turbine is sufficient to accurately describe the relation between wind speed and the turbine output power. The model also shows that under normal system operating conditions, and for the time scales of interest, the interaction between the wind-based electricity source and the network is mainly through its power injection. Letting $w_i(t) \in \mathbb{R}$ denote the representative wind speed for the i^{th} wind power plant at time t, the power injection arising from the renewable plant can be described by

$$\frac{dz_i}{dt} = \alpha_i(z_i, w_i) \tag{2.1a}$$

$$P_i^w = \beta_i(z_i) \tag{2.1b}$$

where $z_i \in \mathbb{R}^{n_i}$ is a vector containing the wind turbine dynamic states, $P_i^w(t)$ is the output power, $\alpha_i : \mathbb{R}^{n_i+1} \mapsto \mathbb{R}^{n_i}$ and $\beta_i : \mathbb{R}^{n_i} \mapsto \mathbb{R}^+$.

2.2 Synchronous Generating Units

For the i^{th} synchronous machine, let δ_i [rad] denote the rotor electrical angular position (with respect to a synchronous reference rotating at ω_s [rad/s]),

ω_i [rad/s] denote the rotor electrical angular velocity, and P_i [pu] denote the turbine power. Let V_i [pu] denote the machine terminal voltage magnitude, and θ_i [rad] denote the machine terminal voltage angle. Let P_i^{ref} [pu] denote the input to the generating unit control logic. Then, the machine dynamics can be described by

$$\begin{aligned}\frac{d}{dt}\begin{bmatrix}\delta_i\\ \omega_i\\ P_i\end{bmatrix} &= \begin{bmatrix}0 & 1 & 0\\ 0 & -\frac{D_i}{M_i} & \frac{1}{M_i}\\ 0 & -\frac{1}{\tau_i R_i \omega_s} & -\frac{1}{\tau_i}\end{bmatrix}\begin{bmatrix}\delta_i\\ \omega_i\\ P_i\end{bmatrix} + \begin{bmatrix}-1\\ \frac{D_i}{M_i}\\ \frac{1}{\tau_i R_i \omega_s}\end{bmatrix}\omega_s \\ &+ \begin{bmatrix}0\\ \omega_i\\ -\frac{E_i V_i}{M_i X_i}\sin(\delta_i - \theta_i)\end{bmatrix} + \begin{bmatrix}0\\ 0\\ \frac{1}{\tau_i}\end{bmatrix} P_i^{ref}\end{aligned} \tag{2.2}$$

where ω_s [rad/s] is the machine electrical synchronous speed, D_i [s/rad] is a damping coefficient, M_i [s^2/rad] is the scaled machine inertia constant, E_i [pu] is the voltage behind reactance (or machine internal voltage), τ_i [s] is the governor time constant, and R_i [pu] is the slope of the machine speed-droop characteristic.

2.3 Network

Standard algebraic power flow equations are used to model the electrical network. For the i^{th} bus, let V_i denote the i^{th} bus voltage magnitude, and let θ_i denote the bus voltage angle. Let P_i^s and Q_i^s denote active and reactive power injections from the i^{th} synchronous generator, and P_i^w denote active power injections from the i^{th} wind power plant. Let P_i^d and Q_i^d denote the active and reactive power demand. Then the power flows equations can be described by

$$P_i^s + P_i^w - P_i^d = \sum_{k=1}^{n} V_i V_k (G_{ik}\cos(\theta_i - \theta_k) + B_{ik}\sin(\theta_i - \theta_k)) \tag{2.3a}$$

$$Q_i^s - Q_i^d = \sum_{k=1}^{n} V_i V_k (G_{ik}\sin(\theta_i - \theta_k) - B_{ik}\cos(\theta_i - \theta_k)) \tag{2.3b}$$

where G_{ik} and B_{ik} are the real and imaginary parts of the network admittance matrix (i,k) entry respectively. We also define $P_{tie\ i}$ as the total real power

exported from area i which is the sum of all outflowing line powers $P_{tie\ i-j}$ to neighboring areas j, i.e.,

$$P_{tie\ i} = \sum_j P_{tie\ i-j} \tag{2.4}$$

where $P_{tie\ i-j}$ is the real power flowing across a lossless line of reactance X_{i-j}; and is given by

$$P_{tie\ i-j} = \frac{|V_i||V_j|}{X_{i-j}} \sin(\delta_i - \delta_j) \tag{2.5}$$

We simplify (2.5) and perturb it to obtain deviations from nominal flow [23]

$$\Delta P_{tie\ i-j} = \frac{377}{X_{i-j}} \int (\Delta\omega_i - \Delta\omega_j) dt \tag{2.6}$$

2.4 Nonlinear Differential-Algebraic Model

The system dynamic behavior can be described by a DAE. The differential part stem from the individual synchronous machine dynamics and the wind power plants as described in (4.1) and (4.1) respectively. The algebraic part results from the network power flow equations and the tie line power interchange as described in (2.3), (2.4) and (2.5). The power output of the wind turbines are treated as a negative load and are taken into account in the computation of the power flow solution of the network. Define the vector of synchronous machine state variables as $x = [x_1', x_2', ..., x_n']'$, with $x_i = [\delta_i, \omega_i, P_i]'$; the vector of synchronous machine power settings as $u = [P_1^{ref}, P_2^{ref}, ..., P_n^{ref}]'$; the vector of tie-line flows as $h = [h_1', h_2', ..., h_m']'$, with $h_i = [P_{i,j}^{tie}]'$ where $j \neq i, j = 1, 2, .., m$ and m is number of neighboring control areas; the vector of algebraic variables as $y = [y_1', y_2', ..., y_n']'$, with $y_i = [\theta_i, V_i]'$; the vector of wind-power-plant generation as $p_w = [P_1^w, P_2^w, ..., P_n^w]'$; the vector of wind-power-plant speed representative wind speeds as $w = [w_1, w_2, ..., w_n]'$; the vector of wind power plant internal variables defining plants power output as $z = [z_1, z_2, ..., z_n]'$; the vector of active power load demands as $p_d = [P_1^d, P_2^d, ..., P_n^d]'$; and the vector of reactive power load demands as $p_q = [P_1^q, P_2^q, ..., P_n^q]'$. Then the

system dynamic behavior can be described by

$$\frac{dx}{dt} = f(x, y, h, u) \tag{2.7a}$$
$$\frac{dz}{dt} = \alpha(z, w) \tag{2.7b}$$
$$p_w = \beta(z) \tag{2.7c}$$
$$h = \phi(x) \tag{2.7d}$$
$$0 = g(x, y, p_d, p_q, p_w) \tag{2.7e}$$

The function $f : \mathbb{R}^{3n} \times \mathbb{R}^{2n} \times \mathbb{R}^m \times \mathbb{R}^n \mapsto \mathbb{R}^n$ results from the synchronous generator dynamics as described in (4.1). The functions $\alpha_i : \mathbb{R}^{n_i+1} \mapsto \mathbb{R}^{n_i}$ and $\beta_i : \mathbb{R}^{n_i} \mapsto \mathbb{R}^+$ result from wind power plant dynamics as described in (4.1). The function $\phi : \mathbb{R}^{3n} \mapsto \mathbb{R}^m$ results from tie-line power interchanges. The function $g : \mathbb{R}^{3n} \times \mathbb{R}^{2n} \times \mathbb{R}^n \times \mathbb{R}^n \times \mathbb{R}^n \mapsto \mathbb{R}^n$ results from the network power flow equations. We assume that the rotor angle of a particular synchronous generator provides the reference and all other rotor angles and bus voltages are defined relative to this reference [20] (Appendix A).

2.5 Linearized Model

We linearize the nonlinear DAE in (2.7) along a nominal trajectory, and use Kron reduction to reduce the resulting linear time-varying (LTV) DAE to an LTV ODE. The nonlinear DAE model in (2.7) includes two inputs (disturbances) that are subject to uncertainty which are the load demand vectors p_d and p_q and the wind-power plant averaged wind speed vector w. These inputs are characterized by their forecast p_d^*, p_q^* and w^*. Assuming the forecast error is small, we linearize the system in (2.7) along a nominal trajectory (x^*, y^*, u^*, h^*) that results from the forecasted p_d^* and w^*. Let $x = x^* + \Delta x$, $y = y^* + \Delta y$, $u = u^* + \Delta u$, $h = h^* + \Delta h$, $p_w = p_w^* + \Delta p_w$, $p_d = p_d^* + \Delta p_d$, $p_q = p_q^* + \Delta p_q$ and $w = w^* + \Delta w$. Then, small variations in system trajectories around (x^*, y^*, h^*, u^*) arising from small variations around p_d^*, p_q^* and w^* can be approximated by

$$\Delta\dot{x} = A_1(t)\Delta x + A_2(t)\Delta y + A_3(t)\Delta h + B_1(t)\Delta u \tag{2.8a}$$
$$\Delta\dot{h} = A_4(t)\Delta x \tag{2.8b}$$

$$\Delta \dot{z} = A_5(t)\Delta z + B_2(t)\Delta w \tag{2.8c}$$

$$\Delta p_w = C_1(t)\Delta z \tag{2.8d}$$

$$0 = C_2(t)\Delta x + C_3(t)\Delta y + D_1(t)\Delta p_d + D_2(t)\Delta p_q + D_3(t)\Delta p_w \tag{2.8e}$$

where

$$\begin{aligned}
A_1(t) &= \frac{\partial f(x,y,h,u)}{\partial x}\Big|_{x^*,y^*,h^*,u^*} & A_2(t) &= \frac{\partial f(x,y,h,u)}{\partial y}\Big|_{x^*,y^*,h^*,u^*} \\
A_3(t) &= \frac{\partial f(x,y,h,u)}{\partial h}\Big|_{x^*,y^*,h^*,u^*} & A_4(t) &= \frac{\partial \phi(x)}{\partial h}\Big|_{x^*} \\
A_5(t) &= \frac{\partial \alpha(z,w)}{\partial z}\Big|_{z^*,w^*} & B_1(t) &= \frac{\partial f(x,y,h,u)}{\partial u}\Big|_{x^*,y^*,h^*,u^*} \\
B_2(t) &= \frac{\partial f(z,w)}{\partial w}\Big|_{z^*,w^*} & C_1(t) &= \frac{\partial \beta(z)}{\partial u}\Big|_{z^*} \\
C_2(t) &= \frac{\partial g(x,y,p_d,p_q,p_w)}{\partial x}\Big|_{x^*,y^*,p_d^*,p_q^*,p_w^*} & C_3(t) &= \frac{\partial g(x,y,p_d,p_q,p_w)}{\partial y}\Big|_{x^*,y^*,p_d^*,p_q^*,p_w^*} \\
D_1(t) &= \frac{\partial g(x,y,p_d,p_q,p_w)}{\partial p_d}\Big|_{x^*,y^*,p_d^*,p_q^*,p_w^*} & D_2(t) &= \frac{\partial g(x,y,p_d,p_q,p_w)}{\partial p_q}\Big|_{x^*,y^*,p_d^*,p_q^*,p_w^*} \\
D_3(t) &= \frac{\partial g(x,y,p_d,p_q,p_w)}{\partial p_w}\Big|_{x^*,y^*,p_d^*,p_q^*,p_w^*}
\end{aligned} \tag{2.9}$$

In (2.8e), if $C_3(t)$ is invertible, we can solve for Δy to obtain

$$\Delta y = -C_3^{-1}(t)[C_2(t)\Delta x + D_1(t)\Delta p_d + D_2(t)\Delta p_q + D_3(t)\Delta p_w] \tag{2.10}$$

$C_3(t)$ is invertible if and only if the power flow Jacobian is invertible. We assume that for the nominal system trajectory $(x^*, y^*, u^*, h^*, p_d^*, p_q^*, p_w^*)$, the power flow equations Jacobian is always invertible. Then we can substitute (2.10) in (2.8a), (2.8b) and (2.8c) to obtain a linear, time-varying ODE model:

$$\begin{aligned}
\frac{d}{dt}\begin{bmatrix}\Delta x\\ \Delta h\\ \Delta z\end{bmatrix} &= \begin{bmatrix}A_{11}(t) & A_{12}(t) & A_{13}(t)\\ A_{21}(t) & A_{22}(t) & A_{23}(t)\\ A_{31}(t) & A_{32}(t) & A_{33}(t)\end{bmatrix}\begin{bmatrix}\Delta x\\ \Delta h\\ \Delta z\end{bmatrix} \\
&\quad + \begin{bmatrix}B_{11}(t) & B_{12}(t) & B_{13}(t)\\ B_{21}(t) & B_{22}(t) & B_{23}(t)\\ B_{31}(t) & B_{32}(t) & B_{33}(t)\end{bmatrix}\begin{bmatrix}\Delta p_d\\ \Delta p_q\\ \Delta w\end{bmatrix} + \begin{bmatrix}\Gamma_1(t)\\ \Gamma_2(t)\\ \Gamma_3(t)\end{bmatrix}\Delta u
\end{aligned} \tag{2.11}$$

with $\Delta x(0) = \Delta h(0) = \Delta z(0) = 0$, and where $A_{11}(t) = A_1(t) - A_2(t)C_3^{-1}(t)C_2(t)$, $A_{12}(t) = A_3(t)$, $A_{13}(t) = -A_2(t)C_3^{-1}(t)D_3(t)C_1(t)$, $A_{22}(t) = A_{23}(t) = A_{31}(t) =$

$A_{32}(t) = 0$, $A_{33}(t) = A_5$, $B_{11}(t) = -A_2(t)C_3^{-1}(t)D_1(t)$,
$B_{12}(t) = -A_2(t)C_3^{-1}(t)D_2(t)$, $B_{13}(t) = -A_2(t)C_3^{-1}(t)D_3(t)$,$B_{21}(t) = B_{23}(t) =$
$B_{23}(t) = B_{31}(t) = B_{32}(t) = 0$, $B_{33}(t) = B_2(t)$, $\Gamma_1(t) = B_1(t)$, $\Gamma_2(t) = \Gamma_3(t) =$
0.

CHAPTER 3

CONTROL STRUCTURE

In this chapter, we consider the model introduced in chapter 2, and provide the background of two potential decentralized controllers for stabilizing the system. We will assume that the set points (x^*, y^*, u^*, h^*) does not change with time; therefore, the linear time-varying ODE in (2.8) reduces to an LTI system of the form

$$\dot{x} = Ax + B_1 d + B_2 u \tag{3.1}$$

where $x = [\Delta x', \Delta h', \Delta z']'$, $d = [\Delta p_d', \Delta p_q', \Delta w']'$, and $u = \Delta u$; and A, B_1, and B_2 are constant matrices.

3.1 Sparsity-Promoting Linear Quadratic Regulator

In [15], the authors develop a method for the design of sparse feedback gains that minimize variance amplification of the distributed system. The method consists of two steps. The first step is to identify a sparsity pattern $\mathcal{S}$ that maintains a balance between the $\mathcal{H}_2$ performance and the sparsity of the controller. This is achieved by introducing sparsity-promoting penalty functions into the optimal control problem. Without the sparsity-promoting functions, the solution to the standard $\mathcal{H}_2$ problem results in centralized controllers with dense feedback gains. Consider the power system model in (3.1) along with

$$z = Cx + Du \tag{3.2}$$

$$u = -Fx \tag{3.3}$$

where z is the performance output, e.g., frequency deviation from its nominal value, $C = \begin{bmatrix} Q^{1/2} & 0 \end{bmatrix}^T$, and $D = \begin{bmatrix} 0 & R^{1/2} \end{bmatrix}^T$, with standard assumptions that (A, B_2) is stabilizable and $(A, Q^{1/2})$ is detectable. The matrix F is a

state feedback gain, $Q = Q^T \geq 0$ and $R = R^T > 0$ are the state and control performance weights, and the closed-loop system is given by

$$\dot{x} = (A - B_2 F)x + B_1 d \tag{3.4}$$

$$C = \begin{bmatrix} Q^{1/2} \\ -R^{1/2}F \end{bmatrix} x \tag{3.5}$$

The authors in [15] introduce the following optimization problem to identify the sparsity pattern $\mathcal{S}$. The objective function of the introduced optimization problem is similar to the standard Linear Quadratic Regulator problem but with an additional term that represents the sparsity of the feedback gains

$$\begin{aligned} &\text{minimize} && J(F) + \gamma g_0(F) \\ &\text{where} && J(F) = \begin{cases} trace((B_1 P(F) B_1), & F \text{ stabilizing} \\ \infty, & \text{otherwise} \end{cases} \\ &\text{and} && g_0(F) = card(F) \end{aligned} \tag{3.6}$$

where $P(F)$ is the closed-loop observability Gramian, which is given by

$$P(F) = \int_0^\infty e^{(A-B_2F)^T t}(Q + F^T R F)e^{(A-B_2F)t} dt \tag{3.7}$$

which can be obtained by solving the corresponding Lyapunov equation

$$(A - B_2 F)^T P + P(A - B_2 F) = -(Q + F^T R F) \tag{3.8}$$

The function card(F) in (3.6) is the cardinality function which calculates the number of nonzero elements in a matrix. The positive scalar γ is used as a weight to characterize the level of sparsity desired in F. We note that $\gamma = 0$ yields a centralized gain which is the solution of the standard LQR problem, i.e., $F_c = R^{-1} B_2^T P$, where P is the unique positive definite solution of the algebraic Riccati equation

$$A^T P + PA + Q - P B_2 R^{-1} B_2^T P = 0 \tag{3.9}$$

After achieving the desired level of sparsity and identifying the sparsity structure $\mathcal{S}$, the authors introduce the second step in the controller design which

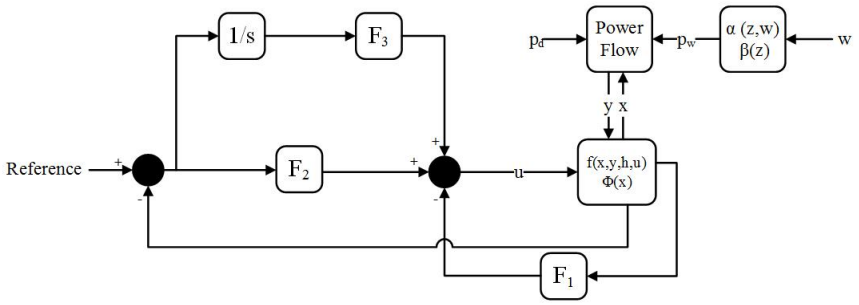

Figure 3.1: Proposed AGC block diagram

involves solving an optimal control problem subject to the feedback gain belonging to the identified structure. This step is important as it can improve the $\mathcal{H}_2$ performance of the structured controller. The optimization problem associated with the second step is

$$\begin{aligned} &\text{minimize} \quad J(F) \\ &\text{subject to} \quad F \in \mathcal{S} \end{aligned} \tag{3.10}$$

For further details of the optimization framework, the reader can refer to [15].

In this thesis, the above control structure will be designed using the information in the linearized augmented model of the power system described in (2.10). We will vary γ until we can find a balance between the performance of the system and the sparsity of the feedback gains. The resulting controller will be applied to the nonlinear DAE system described in (2.7). Looking back again at the objectives of the AGC system, we recall that the main purpose is to maintain the nominal frequency and correct the power interchange between control areas. As a result, it is reasonable to modify the feedback control loop to put more emphasis on the states resembling the control area frequency and the tie-line. In addition, we add integrators to those states to reset them to their nominal values after being subjected to a load change or a wind disturbance. Furthermore, for simulation purposes and to create an environment similar to real life power systems, a power flow program is run at each AGC cycle to update the algebraic variables in the closed-loop and account for the network dynamics. Figure. 3.1 shows a block diagram of the proposed feedback control structure. From the figure, F_2 are gains associated with the states corresponding to the area frequency and the

tie-line power interchange, F_3 are gains associated with the integral of the above states and F_1 are gains are associated with the rest of the states. Our goal is to have F_1 and F_2 as sparse as possible; hence, we will design them using the sparsity-promoting linear quadratic regulator method introduced in this section. F_3 will be designed using the traditional linear quadratic regulator method rather than the sparsity-promoting linear quadratic regulator method because the states associated with F_3 impose constraints on the optimization problem rendering it unsolvable.

3.2 Decentralized Overlapping Control Using Linear Quadratic State Feedback

The non-linear differential algebraic model of the power system described in (2.7) consists of overlapping subsystems (control areas) that share common parts (tie-lines). We employ the theory of overlapping control to expand the power system model into subsystems that belong to the same control area, and then design a local controller for each area. The decentralized control laws obtained in the expanded space are contracted back to the original space to be applied on the power system in (2.7). This method reduces the computational complexity of designing a single centralized feedback controller for a large power system to the design of local controllers for small subsystems. In addition, this method improves the reliability of the control system as it stabilizes subsystems to ensure the stability of the whole system. As a result, failure of a subsystem or part of a subsystem does not affect the stability of other subsystems.

The method of overlapping control relies on the inclusion principle for linear systems. The inclusion principle provides conditions for which the trajectories of the original system $\mathbf{S}$ are included in the set of trajectories of the expanded system $\tilde{\mathbf{S}}$ [17], [24], [25]. Consider the systems

$$\begin{aligned} \mathbf{S}: &\ \dot{x} = Ax + Bu,\ x(t_0) = x_0 \\ \tilde{\mathbf{S}}: &\ \dot{\tilde{x}} = \tilde{A}\tilde{x} + \tilde{B}\tilde{u},\ \tilde{x}(t_0) = \tilde{x}_0 \end{aligned} \tag{3.11}$$

with $\tilde{n} > n$ and $\tilde{m} > m$. The term $x(t; x_0, u)$ denotes trajectories of system $\mathbf{S}$ while $\tilde{x}(t; \tilde{x}_0, \tilde{u})$ denotes trajectories of system $\tilde{\mathbf{S}}$. Assume that there exists

the following pair of expansion/contraction matrices for the state:

$$V \in \mathbb{R}^{\tilde{n}\times n},\ U \in \mathbb{R}^{n\times\tilde{n}},\ UV = I \in \mathbb{R}^{\tilde{n}\times n} \tag{3.12}$$

and, respectively, for the input:

$$R \in \mathbb{R}^{\tilde{m}\times m},\ U \in \mathbb{R}^{m\times\tilde{m}},\ QR = I \in \mathbb{R}^{\tilde{m}\times m} \tag{3.13}$$

According to [24] it can be shown that system $\tilde{\mathbf{S}}$ includes system $\mathbf{S}$ if for any initial state x_0 and any input $u(t)$, we have $x(t; x_0, u) = U\tilde{x}(t; Vx_0, Ru)$. In addition, system $\tilde{\mathbf{S}}$ includes system $\mathbf{S}$ if and only if $A^i = U\tilde{A}^iV$ and $A^iB = U\tilde{A}^i\tilde{B}R$ for $i \in \{0, 1, ..., \tilde{n} - 1\}$. Assume the static feedback control laws for both systems to be in the following form:

$$\begin{aligned} u &= Fx,\ F \in \mathbb{R}^{m\times n} \\ \tilde{u} &= \tilde{F}\tilde{x},\ \tilde{F} \in \mathbb{R}^{\tilde{m}\times\tilde{n}} \end{aligned} \tag{3.14}$$

Then the closed-loop systems in the original space and the expanded space take the following form:

$$\begin{aligned} \bar{\mathbf{S}} &: \dot{x} = (A + BF)x \\ \bar{\tilde{\mathbf{S}}} &: \dot{\tilde{x}} = (\tilde{A} + \tilde{B}\tilde{F})\tilde{x} \end{aligned} \tag{3.15}$$

It can be shown [24] that $\bar{\mathbf{S}}$ is a restriction of $\bar{\tilde{\mathbf{S}}}$ if one of the following is true:

$$\tilde{A}V = VA \text{ and } \tilde{B}R = VB, \text{ and } \tilde{F}V = RF \tag{3.16a}$$

$$\tilde{A}V = VA \text{ and } \tilde{B} = VBQ, \text{ and } F = Q\tilde{F}V \tag{3.16b}$$

For an overlapping interconnected system, expanding the system to a higher dimensional space can be done by repeating the overlapping parts to produce decoupled subsystems. For our case where we have a DAE model of a power system, the linearized model in (2.10) is expanded to from decoupled subsystems. The expansion is carried over by repeating the states corresponding to the tie-line flows for each control area. For example, if we have a two-control area power system, then the expansion is carried out as

follows:

$$\begin{bmatrix} \Delta\tilde{x} \\ \Delta\tilde{h} \\ \Delta\tilde{z} \end{bmatrix} = V \begin{bmatrix} \Delta x \\ \Delta h \\ \Delta z \end{bmatrix} = \begin{bmatrix} I_1 & 0 & 0 \\ 0 & I_2 & 0 \\ 0 & I_2 & 0 \\ 0 & 0 & I_3 \end{bmatrix} \begin{bmatrix} \Delta x \\ \Delta h \\ \Delta z \end{bmatrix} \tag{3.17}$$

where I_1, I_2 and I_3 are identity matrices with dimensions corresponding to the vector components of Δx, Δh and Δz. In the expanded space, controllers are designed to stabilize each subsystem i (each control area) using the theory of linear quadratic control, where each controller $\tilde{F}_i$ is defined as $\tilde{F}_i = \tilde{R}_i^{-1}\tilde{B}_{2i}^T\tilde{P}_i$ following what we described earlier in (3.2), (3.4) and (3.9). This way each control area depends only on the local states plus the state describing the change in tie-line power. The designed controllers in the expanded space, i.e. $\tilde{F}$. are contracted back to the original space using the relations from the inclusion principle. Similar to what we did in Section 3.1, a power flow program is run at each AGC cycle to update the algebraic variables in the closed-loop and account for the network dynamics. The feedback control structure shown in Figure. 3.1 is again used to implement the designed controller.

CHAPTER 4

3-MACHINE 9-BUS 2-RENEWABLE RESOURCES CASE STUDY

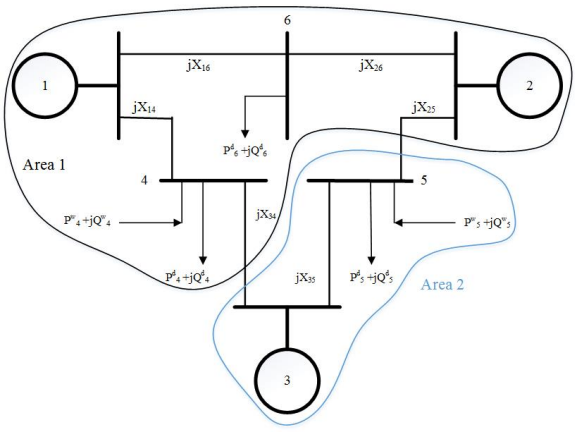

Figure 4.1: 3-machine, 6-bus system with 2 balancing areas

In this chapter, the theory presented in the previous chapters is illustrated with the 3-machine, 6-bus system of Figure 4.1, which is an adaption of the 3-machine, 9-bus model of the Western System Coordinating Council (WECC) system [20]. We introduce wind power plants at buses 4 and 5. Two balancing areas are considered as shown in the figure. The following is a breakdown of the model and parameters used to simulate this case

4.1 Power System Model

4.1.1 Wind-Based Electricity Resource Model

Following what we described in (2.7a), we use a first-order aggregate wind farm reduced-order model presented in [22] which closely resembles the impact of wind turbine generators in a power system. As a result, the model

in Section 2.1 is reduced to

$$\frac{dz_i}{dt} = -0.0783 z_i + 0.0058 w_i - 0.0467 \tag{4.1a}$$

$$P_i^w = z_i \tag{4.1b}$$

4.1.2 Synchronous Generators

Following what we described in (2.7a), we have for this case $x = [x_1, x_2, x_3]'$ with $x_i = [\delta_i, w_i, P_i]'$, $y = [y_1, y_2, y_3, y_4, y_5, y_6]'$ with $y_i = [\theta_i, V_i]'$, and $u = [P_1^{ref}, P_2^{ref}, P_3^{ref}]'$. We use the machine parameters in Table 4.1 which is adapted from example 7.1 in [20].

Table 4.1: Machine Data

Parameters	Machine 1	Machine 2	Machine 3
$M\ [s^2/rad]$	0.019	0.034	0.016
$D\ [s/rad]$	0.0019	0.0034	0.0016
$R\ [pu]$	0.05	0.05	0.05
$\tau\ [s]$	0.2	0.2	0.2
$X_d\ [pu]$	0.2	0.2	0.2

4.1.3 Network

Following what we described in Section 2.3, we have for this case $p_d = [p_4^d, p_5^d, p_6^d]'$ and $p_w = [p_4^w, p_5^w]'$. Let $Y_{ik} = 1/X_{ik}$ be the admittance of the transmission line between buses i and k; then we have the following algebraic power flow equations:

Power balance equations for bus 1

$$\begin{aligned} \frac{E_1 V_1}{X_1}\sin(\delta_1 - \theta_1) &= Y_{14} V_1 V_4 \sin(\theta_1 - \theta_4) + Y_{16} V_1 V_6 \sin(\theta_1 - \theta_6) \\ \frac{E_1 V_1}{X_1}\cos(\delta_1 - \theta_1) &= -Y_{14} V_1 V_4 \cos(\theta_1 - \theta_4) - Y_{16} V_1 V_6 \cos(\theta_1 - \theta_6) \\ &\quad + (Y_{14} + Y_{16} + Y_1) V_1^2 \end{aligned} \tag{4.2}$$

Power balance equations for bus 2

$$\begin{aligned}\frac{E_2V_2}{X_2}\sin(\delta_2-\theta_2) &= Y_{25}V_2V_5\sin(\theta_2-\theta_5)+Y_{26}V_2V_6\sin(\theta_2-\theta_6)\\ \frac{E_2V_2}{X_2}\cos(\delta_2-\theta_2) &= -Y_{25}V_2V_5\cos(\theta_2-\theta_5)+Y_{26}V_2V_6\cos(\theta_2-\theta_6)\\ &\quad +(Y_{25}+Y_{26}+Y_2)V_2^2\end{aligned} \tag{4.3}$$

Power balance equations for bus 3

$$\begin{aligned}\frac{E_3V_3}{X_3}\sin(\delta_3-\theta_3) &= Y_{34}V_3V_4\sin(\theta_3-\theta_4)+Y_{35}V_3V_5\sin(\theta_3-\theta_5)\\ \frac{E_3V_3}{X_3}\cos(\delta_3-\theta_3) &= -Y_{34}V_3V_4\cos(\theta_3-\theta_4)-Y_{35}V_3V_5\cos(\theta_3-\theta_5)\\ &\quad +(Y_{34}+Y_{35}+Y_3)V_3^2\end{aligned} \tag{4.4}$$

Power balance equations for bus 4

$$\begin{aligned}P_4^w-P_4^d &= Y_{14}V_4V_1\sin(\theta_4-\theta_1)+Y_{34}V_4V_3\sin(\theta_3-\theta_4)\\ -Q_4^d &= -Y_{14}V_4V_1\cos(\theta_4-\theta_1)-Y_{34}V_4V_3\cos(\theta_4-\theta_3)+(Y_{14}+Y_{34})V_4^2\end{aligned} \tag{4.5}$$

Power balance equations for bus 5

$$\begin{aligned}P_5^w-P_5^d &= Y_{25}V_5V_2\sin(\theta_5-\theta_2)+Y_{35}V_3V_5\sin(\theta_5-\theta_3)\\ -Q_5^d &= -Y_{25}V_5V_2\cos(\theta_5-\theta_2)-Y_{35}V_5V_3\cos(\theta_5-\theta_3)+(Y_{25}+Y_{35})V_5^2\end{aligned} \tag{4.6}$$

Power balance equations for bus 6

$$\begin{aligned}-P_6^d &= Y_{16}V_6V_1\sin(\theta_6-\theta_1)+Y_{26}V_6V_2\sin(\theta_6-\theta_2)\\ -Q_6^d &= -Y_{16}V_6V_1\cos(\theta_6-\theta_1)-Y_{26}V_6V_2\cos(\theta_6-\theta_2)+(Y_{16}+Y_{26})V_6^2\end{aligned} \tag{4.7}$$

The network parameters are found in Table 4.2

Table 4.2: Line Admittance in pu

Y_{14}	Y_{16}	Y_{25}	Y_{26}	Y_{34}	Y_{35}
6.21	13.90	5.88	9.92	11.76	10.87

In addition, the change in tie-line power for this case is

$$\Delta P_{tie\ 1-2} = \frac{377}{X_{1-2}}\int(\Delta\omega_1+\Delta\omega_2-\Delta\omega_3)dt \tag{4.8}$$

where X_{1-2} is the reactance of the tie-line between areas 1 and 2. The resulting matrices A, B_1, and B_2 of (3.1) formed by the model can be found in Appendix B.

4.2 Sparsity-Promoting Linear Quadratic Regulator

The linearized DAE power system has now the following form according to what we described in (2.8). To recapitulate what we stated in Chapter 3, we will assume that the set points (x^*, y^*, u^*, h^*) does not change with time; therefore, the linear time-varying ODE in (2.8) reduces to an LTI system of the form

$$\dot{x} = Ax + B_1 d + B_2 u \tag{4.9}$$

where $x = [\Delta x', \Delta h', \Delta z']'$, $d = [\Delta p_d', \Delta p_q', \Delta w']'$, and $u = \Delta u$; and A, B_1, and B_2 are constant matrices. In this section, our controller is designed to be in the form

$$\dot{v} = \begin{bmatrix} \Delta\omega_1 \\ \Delta\omega_2 \\ \Delta\omega_3 \\ \Delta P_{tie\ 1-2} \end{bmatrix} \tag{4.10}$$

$$u = Fx + Kv \tag{4.11}$$

where F is designed using the sparsity-promoting control algorithm and K is designed using nominal LQR method.

We used the MATLAB code for "Design of optimal sparse feedback gains" written by the authors of [26] to calculate the sparse gains for the controller in Section 3.1 for different values of γ using the information from the linear DAE model in Section 4.1. Two different values of γ were used to promote the sparsity of the controller gain. The first value is $\gamma = 100$ which yielded a gain F that has 23 zeros out of 33 entries. The other value is $\gamma = 1000$ which yielded a gain F that has 25 zeros out of 33 entries. Note that the $\gamma = 100$ yielded the maximum sparsity achievable using this method for this power system case. The results show that for the case where $\gamma = 1000$, the states that needed to be transported across the control areas are δ_2, δ_3, $\int \omega_1$,

$\int \omega_2$, $\int \omega_3$ and $\int P_{tie}$ only. While for $\gamma = 1000$ the states that needed to be transported across the control areas are δ_3, $\int \omega_1$, $\int \omega_2$, $\int \omega_3$ and $\int P_{tie}$ only. The calculated gains are

$$F_{\gamma=100} = \begin{bmatrix} 12.40 & 7.11 & 0 & 0 & 0 & -12.66 & 0 & 0 & -8.88 & 0 & 0 \\ 0 & 0 & 0 & 10.633 & 10.28 & 6.70 & 0 & 0 & 0 & 0 & 0 \\ 0 & 0 & 7.10 & 0 & 0 & 98.21 & 11.31 & 15.90 & 0 & 0 & 0 \end{bmatrix} \tag{4.12}$$

$$F_{\gamma=1000} = \begin{bmatrix} 17.53 & 0 & 0 & 0 & 0 & -12.54 & 0 & 0 & 0 & 0 & 0 \\ 0 & 0 & 0 & 10.56 & 10.41 & 7.42 & 0 & 0 & 0 & 0 & 0 \\ 0 & 0 & 0 & 0 & 0 & 99.45 & 11.35 & 15.97 & 0 & 0 & 0 \end{bmatrix} \tag{4.13}$$

Table 4.3 shows the different values of γ used and the corresponding percentage of sparsity achieved.

Table 4.3: Percentage of Sparsity for Each Controller

	Sparsity-Promoting Control	
γ	100	1000
Percentage	51.11%	55.56%

4.2.1 25% Wind Energy Penetration

In this section, we use Simulink to build and simulate the non-linear DAE presented in Sections 4.1 and 4.2. We assumed that wind energy accounts for 25% of the generation at the beginning of the simulation. Then at $t = 10$ s the system loses its wind generation part. At $t = 20$ s, wind generation regains its 25% share, then loses it again at $t = 30$ s and gains it back at $t = 40$ s. The purpose of this scenario is to show how the controller responds to this abrupt change in generation, and to try to simulate the worst case scenario of unpredictable wind speeds. We set the scheduled power interchange to be 0.5 pu. For the sake of comparison, the gains of the centralized controller were calculated using the theory of linear qaudratic control. Figure 4.2(a)–4.3(c) show the evolution of the frequency of the three machines for the (i) centralized controller, (ii) the sparsity-promoting controller with $\gamma = 100$,

and (iii) the sparsity-promoting controller with $\gamma = 1000$. Figure 4.3(d) shows the response of the tie line power flows for the For the same scenario described above.

We see that as the wind power generation is connected and disconnected through the simulation, the frequency is stabilized in minimal time with minimum overshoot. Comparing the controllers designed using the sparsity-promoting linear quadratic regulator to the centralized controller, we see from Figure 4.2(a)–4.3(d) that the performance of the controller corresponding to $\gamma = 1000$ is very close (almost identical) to the performance of the centralized controller. The controller corresponding to $\gamma = 1000$ (more decentralization) has a slightly larger overshoot and a slower settling time.

4.2.2 50% Wind Energy Penetration

In this section, we assume that wind energy accounts for 50% of the generation at the beginning of the simulation. We repeat the same scenario from the previous section where at $t = 10$ s the system loses its wind generation part. At $t = 20$ s, wind generation regains its 20% share, then loses it again at $t = 30$ s and gains it back at $t = 40$ s. The purpose of this scenario is to show how the controller responds to this abrupt change in generation, and to try to simulate the worst case scenario of unpredictable wind speeds. We set the scheduled power interchange between to be 0.5 pu. For the sake of comparison, the gains of a centralized controller were calculated using the theory of linear quadratic control. Figure 4.3(a)–4.4(c) show the evolution of the frequency of the three machines for the (i) centralized controller, (ii) the sparsity-promoting controller with $\gamma = 100$, and (iii) the sparsity-promoting controller with $\gamma = 1000$. Figure 4.4(d) shows the response of the tie line power flows for the same scenario described above.

We see that as the wind power generation is connected and disconnected through the simulation, the frequency is stabilized in minimal time with minimum overshoot. Comparing the controllers designed using the sparsity-promoting linear quadratic regulator to the centralized controller, we see from Figure 4.3(a)–4.4(d) that the performance of the controller corresponding to $\gamma = 1000$ is very close (almost identical) to the performance of the centralized controller. The controller corresponding to $\gamma = 1000$ (more decentralization)

has a slightly larger overshoot and a slower settling time.

4.3 Decentralized Overlapping Control Using Linear Quadratic State Feedback

The linearized DAE power system now has the following form according to what we described in (2.8). To recapitulate what we stated in Chapter 3, we will assume that the set points (x^*, y^*, u^*, h^*) does not change with time; therefore, the linear time-varying ODE in (2.8) reduces to an LTI system of the form

$$\dot{x} = Ax + B_1 d + B_2 u \tag{4.14}$$

where $x = [\Delta x', \Delta h', \Delta z']'$, $d = [\Delta p_d', \Delta p_q', \Delta w']'$, and $u = \Delta u$; and A, B_1, and B_2 are constant matrices. In this section, our controller is designed to be in the form

$$\dot{v} = \begin{bmatrix} \Delta\omega_1 + \Delta P_{tie\ 1-2} \\ \Delta\omega_2 + \Delta P_{tie\ 1-2} \\ \Delta\omega_3 - \Delta P_{tie\ 1-2} \end{bmatrix} \tag{4.15}$$

$$u = Fx + Kv = \begin{bmatrix} F & K \end{bmatrix} \begin{bmatrix} x \\ v \end{bmatrix} \tag{4.16}$$

where $[F\ K]$ is designed using overlapping control method.

The system in (2.10) along with (4.15) is expanded to allow for the design of the decentralized controller. The expansion is carried out by repeating the tie-lie state 3 times to reflect the 3 subsystems corresponding to the 3 machines. As a result, for this case, the states in the expanded space have

the following form:

$$\begin{bmatrix} \Delta\tilde{x} \\ \Delta\tilde{h} \\ \Delta\tilde{z} \\ \Delta\tilde{v} \end{bmatrix} = V \begin{bmatrix} \Delta x \\ \Delta h \\ \Delta z \\ \Delta v \end{bmatrix} = \begin{bmatrix} I_{9\times9} & 0 & 0 & 0 \\ 0 & I_{1\times1} & 0 & 0 \\ 0 & I_{1\times1} & 0 & 0 \\ 0 & I_{1\times1} & 0 & 0 \\ 0 & 0 & I_{2\times2} & 0 \\ 0 & 0 & 0 & I_{3\times3} \end{bmatrix} \begin{bmatrix} \Delta x \\ \Delta h \\ \Delta z \\ \Delta v \end{bmatrix} \tag{4.17}$$

Consequently, the expanded system matrices have the following form according to (3.16):

$$\tilde{A}V = VA \text{ and } \tilde{B} = VBQ \tag{4.18}$$

where $Q = I_{3\times3}$. Next the 3 subsystems are separated to design the local LQR controllers. Since the tie-line state is repeated 3 times in the expanded space, each subsystem will assume it has its own tie-line state. In addition, since the coupling between the wind turbines and the machines is weak, we will assume that the wind turbines do not belong to any system. As a result, no information from the wind turbines is needed for state feedback. The separation is done by extracting the information of each subsystem from the system matrices A and B. As a result, the subsystems have the following form:

$$\frac{d}{dt} \begin{bmatrix} \Delta x_i \\ \Delta h_i \\ \Delta v_i \end{bmatrix} = \Phi_i \begin{bmatrix} \Delta x_i \\ \Delta h_i \\ \Delta v_i \end{bmatrix} + \Pi_i \begin{bmatrix} \Delta p_d \\ \Delta p_q \end{bmatrix} + \Xi_i \Delta u_i \tag{4.19}$$

where Φ_i, Π_i and Ξ_i are extracted from (2.10) along with (4.15) using the information in Appendix B to reflect the case example we are simulating. As a result, we have the following for each subsystem:
Subsystem 1

$$\Phi_1 = \begin{bmatrix} -0.10 & 7.97 & -3.99 & 0 \\ -0.27 & -5 & 0 & 0 \\ 0.86 & 0 & 0 & 0 \\ 1 & 0 & 1 & 0 \end{bmatrix}, \Xi_1 = \begin{bmatrix} 0 \\ 5 \\ 0 \\ 0 \end{bmatrix} \tag{4.20}$$

Subsystem 2

$$\Phi_2 = \begin{bmatrix} 0 & 1 & 0 & 0 & 0 \\ 2.56 & -0.2 & 29.45 & -14.73 & 0 \\ 0 & -0.27 & -5 & 0 & 0 \\ 0 & 0.86 & 0 & 0 & 0 \\ 0 & 1 & 0 & 1 & 0 \end{bmatrix}, \Xi_2 = \begin{bmatrix} 0 \\ 0 \\ 5 \\ 0 \\ 0 \end{bmatrix} \tag{4.21}$$

Subsystem 3

$$\Phi_3 = \begin{bmatrix} 0 & 1 & 0 & 0 & 0 \\ 417.19 & -0.3 & 62.62 & 62.62 & 0 \\ 0 & -0.27 & -5 & 0 & 0 \\ 0 & -1.73 & 0 & 0 & 0 \\ 0 & 1 & 0 & -1 & 0 \end{bmatrix}, \Xi_3 = \begin{bmatrix} 0 \\ 0 \\ 5 \\ 0 \\ 0 \end{bmatrix} \tag{4.22}$$

For each subsystem, we design an LQR controller that is computed using MATLAB (Appendix C).
Subsystem 1

$$Q_1 = 100 \times I_{4\times4}, R_1 = I_{1\times1}, F_1 = \begin{bmatrix} 11.89 & 10.79 & 5.79 & 10 \end{bmatrix} \tag{4.23}$$

Subsystem 2

$$Q_2 = \begin{bmatrix} 0.5 & 0 & 0 & 0 & 0 \\ 0 & 5 & 0 & 0 & 0 \\ 0 & 0 & 0.5 & 0 & 0 \\ 0 & 0 & 0 & 5 & 0 \\ 0 & 0 & 0 & 0 & 5 \end{bmatrix}, R_2 = I_{1\times1}, F_2 = \begin{bmatrix} 0.48 & 2.41 & 4.47 & -0.23 & 2.23 \end{bmatrix} \tag{4.24}$$

Subsystem 3

$$Q_3 = 40 \times I_{4\times4}, R_3 = I_{1\times1}, F_3 = \begin{bmatrix} 108.89 & 9.02 & 15.34 & -1.47 & 6.32 \end{bmatrix} \tag{4.25}$$

Next we join F_1, F_2 and F_3 to get $\tilde{F}$, and use the equation $F = Q\tilde{F}V$ from (3.16) to get F:

$$\tilde{F} = \begin{bmatrix} 11.89 & 10.79 & 0 & 0 & 0 & 0 & 0 & 0 & 5.79 & 0 & 0 & 0 & 0 & 10 & 0 & 0 \\ 0 & 0 & 0.48 & 2.40 & 4.47 & 0 & 0 & 0 & 0 & -0.23 & 0 & 0 & 0 & 0 & 2.23 & 0 \\ 0 & 0 & 0 & 0 & 0 & 108.89 & 9.02 & 15.34 & 0 & 0 & -1.47 & 0 & 0 & 0 & 0 & 6.32 \end{bmatrix} \tag{4.26}$$

$$F = \begin{bmatrix} 11.89 & 10.79 & 0 & 0 & 0 & 0 & 0 & 0 & 5.79 & 0 & 0 & 10 & 0 & 0 \\ 0 & 0 & 0.48 & 2.40 & 4.47 & 0 & 0 & 0 & -0.23 & 0 & 0 & 0 & 2.23 & 0 \\ 0 & 0 & 0 & 0 & 0 & 108.89 & 9.02 & 15.34 & -1.47 & 0 & 0 & 0 & 0 & 6.32 \end{bmatrix} \tag{4.27}$$

We note from F that only the P_{tie} state is needed by both control areas. We also note that control areas depend only on local measurements to implement the LQR controller. The designed overlapping controller F has 28 zeros out of 42 entries yielding a 66.67% sparsity. The resulting controller provides more decentralization than the controllers designed using the method of Section 4.2 as seen in Table 4.4.

Table 4.4: Percentage of Sparsity for Each Controller

	Sparsity-Promoting Control		Overlapping Control
γ	100	1000	-
Percentage	51.11%	55.56%	66.67%

4.3.1 25% Wind Energy Penetration

In this section, we use Simulink to build and simulate the non-linear DAE presented in Sections 4.1 and 4.3. We assumed that wind energy accounts for 25% of the generation at the beginning of the simulation. Then at $t = 30$ s the system loses its wind generation part. At $t = 40$ s, wind generation regains its 25% share, then loses it again at $t = 50$ s and gains it back at $t = 60$ s. The purpose of this scenario is to show how the controller responds to this abrupt change in generation, and to try to simulate the worst case scenario of unpredictable wind speeds. We set the scheduled power interchange to be 0.5 pu. Figures 4.4(a)–4.5(d) show the dynamics of the frequency of the three machines and the response of the tie-line flows for the (i) centralized controller, (ii) the sparsity-promoting controller with $\gamma = 1000$, and (iii)

the decentralized overlapping controller. From the figures we see that the controller corresponding to overlapping control (more decentralization) has a slower response time initially among the other two controllers, but after settling to the desired frequency, the decentralized overlapping controller responds very similarly to the centralized controller and to the less sparsity-promoting controller but with a slightly larger overshoot.

4.3.2 50% Wind Energy Penetration

In this section, we assume that wind energy accounts for 50% of the generation at the beginning of the simulation. We repeat the same scenario from the previous section where at $t = 30$ s the system loses its wind generation part. At $t = 40$ s, wind generation regains its 20% share, then loses it again at $t = 50$ s and gains it back at $t = 60$ s. The purpose of this scenario is to show how the controller responds to this abrupt change in generation, and to try to simulate the worst case scenario of unpredictable wind speeds. We set the scheduled power interchange to be 0.5 pu. For the sake of comparison, the gains of a centralized controller were calculated using the theory of linear quadratic control. Figure 4.5(a)–4.6(c) show the evolution of the frequency of the three machines for the (i) centralized controller, (ii) the sparsity-promoting controller with $\gamma = 1000$, and (iii) the decentralized overlapping controller. Figure 4.6(d) shows the response of the tie line power flows for the same scenario described above.

We see that as the wind power generation is connected and disconnected through the simulation, the frequency is stabilized in minimal time with minimum overshoot. The controller designed using overlapping control (more decentralization) has a slower response time initially than the other two controllers, but after settling to the desired frequency, the decentralized overlapping controller responds very similarly to the centralized controller and to the less sparsity-promoting controller but with a slightly larger overshoot.

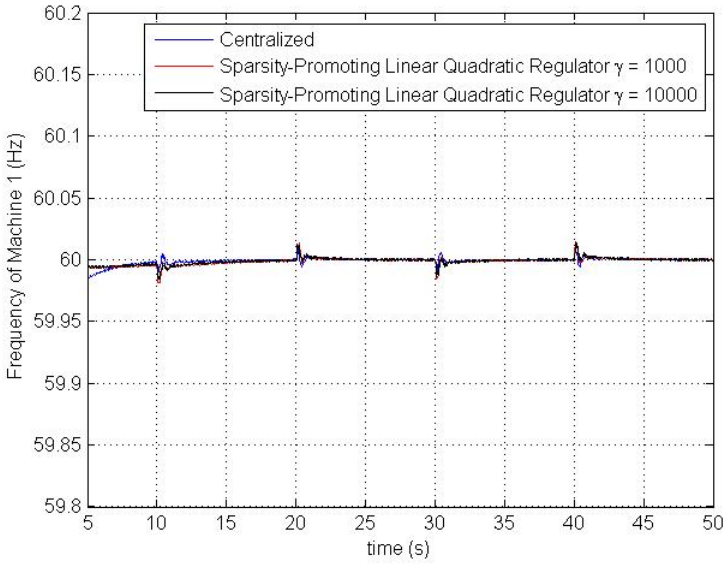

(a) Frequency Response of Machine 1

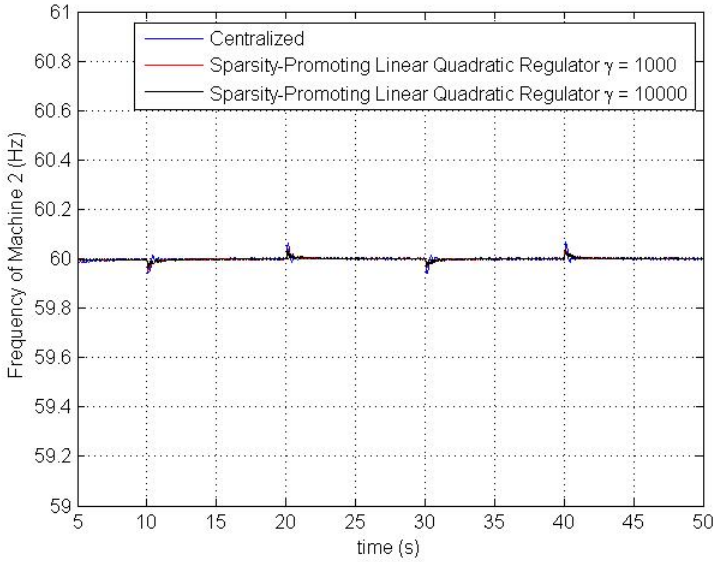

(b) Frequency Response of Machine 2

Figure 4.2: Subfigures (a) (b) and (c) display how the frequencies of machines 1, 2 and 3 respectively change when the wind generation changes at $t = 10$ s, $t = 20$ s, $t = 30$ s and $t = 40$ s. Subfigure (d) displays tie-line flows across the two areas for the same disturbances. The plots show the response when the following controllers are employed: centralized controller, sparsity-promoting linear quadratic controller with $\gamma = 100$, sparsity-promoting linear quadratic controller with $\gamma = 1000$.

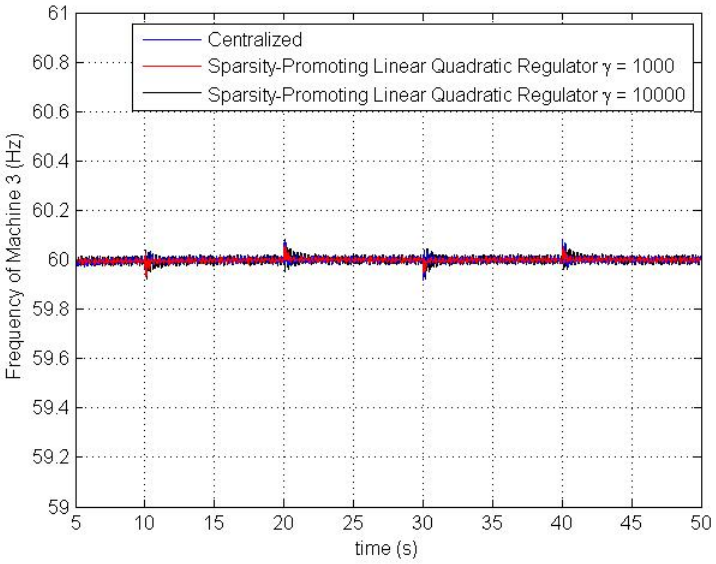

(c) Frequency Response of Machine 3

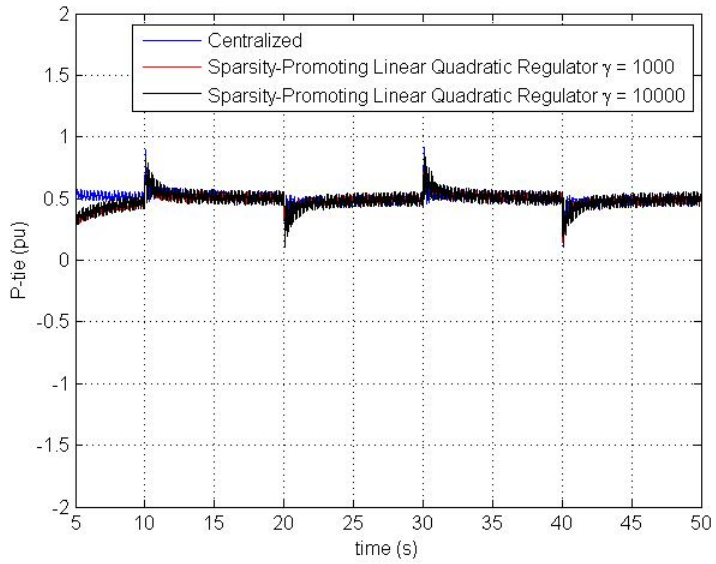

(d) Dynamic Response of tie-line flows across areas 1 and 2

Figure 4.2: Continued.

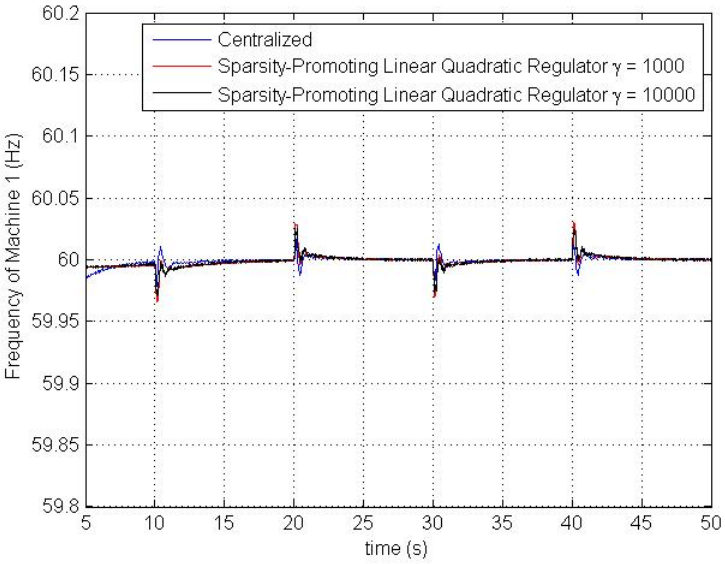

(a) Frequency Response of Machine 1

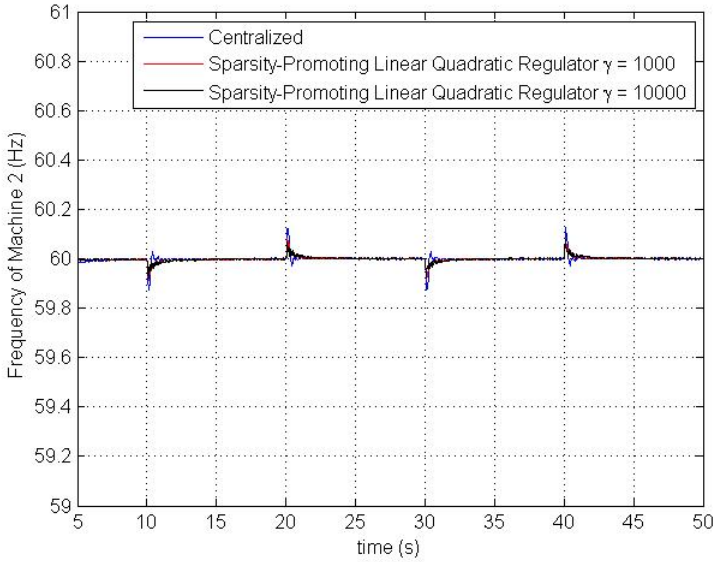

(b) Frequency Response of Machine 2

Figure 4.3: Subfigures (a) (b) and (c) display how the frequencies of machines 1, 2 and 3 respectively change when the wind generation changes at $t = 10$ s, $t = 20$ s, $t = 30$ s and $t = 40$ s. Subfigure (d) displays tie-line flows across the two areas for the same disturbances. The plots show the response when the following controllers are employed: centralized controller, sparsity-promoting linear quadratic controller with $\gamma = 100$, sparsity-promoting linear quadratic controller with $\gamma = 1000$.

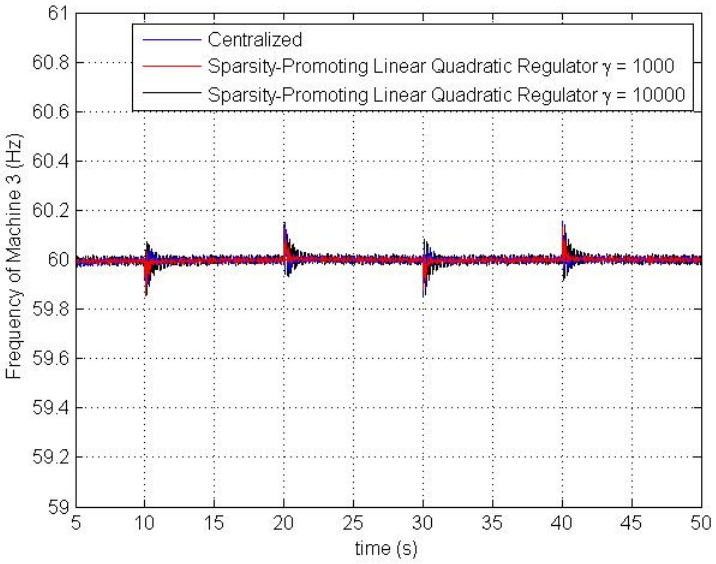

(c) Frequency Response of Machine 3

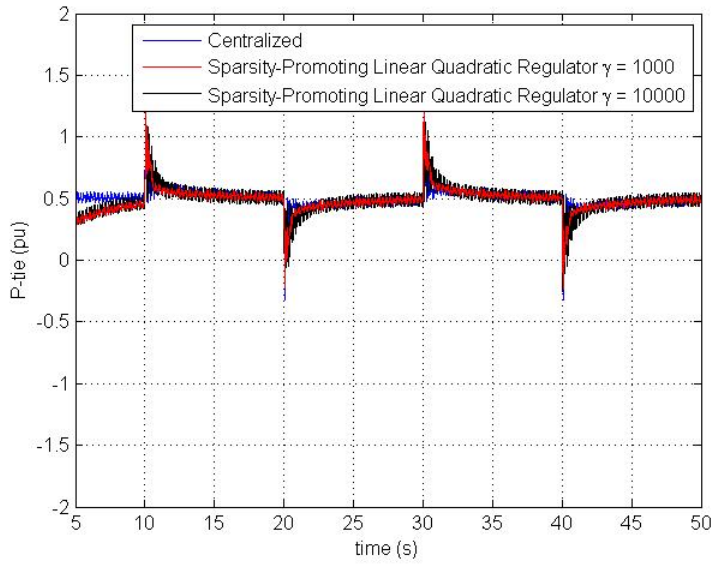

(d) Dynamic Response of tie-line flows across areas 1 and 2

Figure 4.3: Continued.

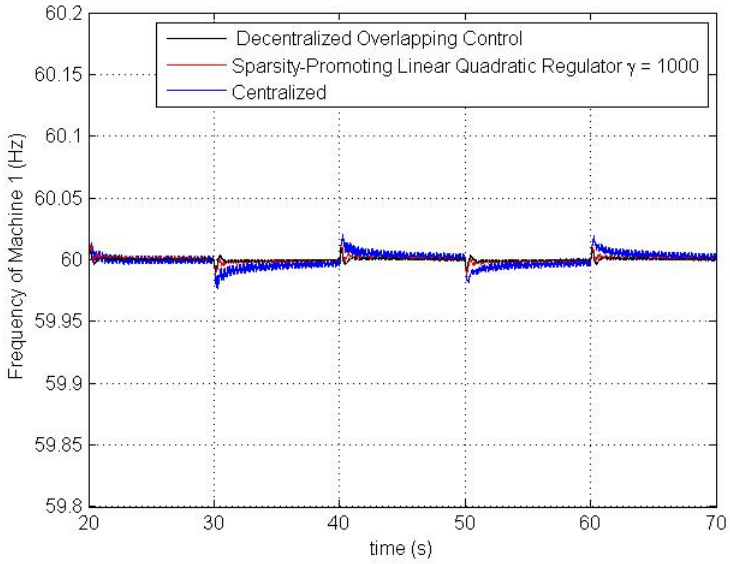

(a) Frequency Response of Machine 1

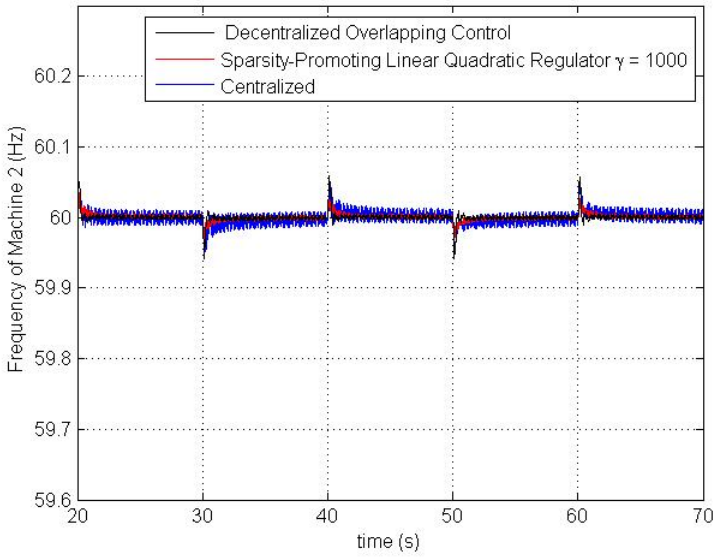

(b) Frequency Response of Machine 2

Figure 4.4: Subfigures (a) (b) and (c) display how the frequency of machines 1, 2 and 3 respectively change when the wind generation changes at $t = 30$ s, $t = 40$ s, $t = 50$ s and $t = 60$ s. Subfigure (d) displays tie-line flows across the two areas for the same disturbances. The plots show the response when the following controllers are employed: centralized controller, sparsity-promoting linear quadratic controller with $\gamma = 1000$, decentralized overlapping controller.

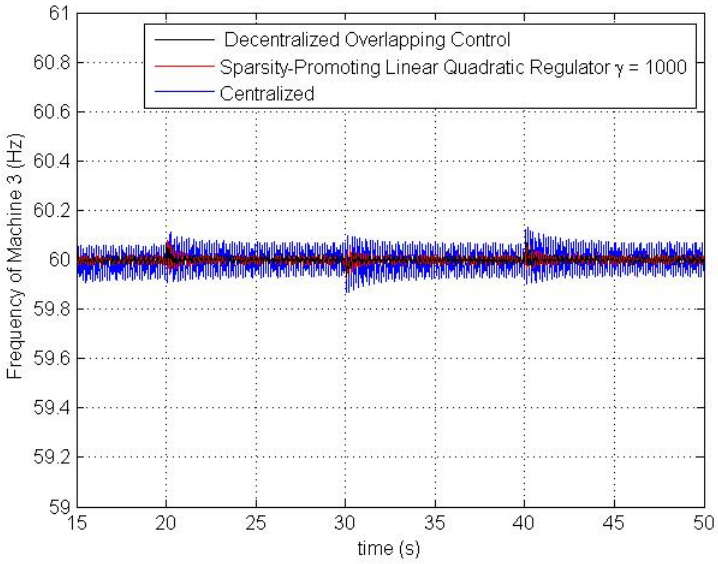

(c) Frequency Response of Machine 3

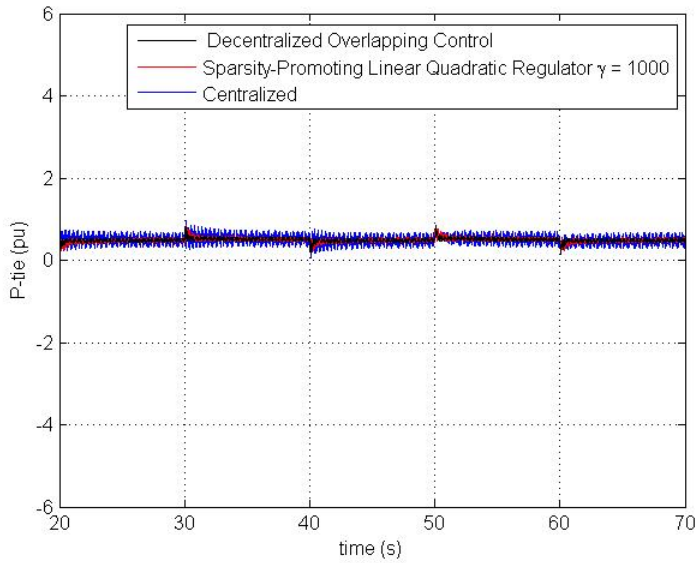

(d) Dynamic Response of tie-line flows across areas 1 and 2

Figure 4.4: Continued.

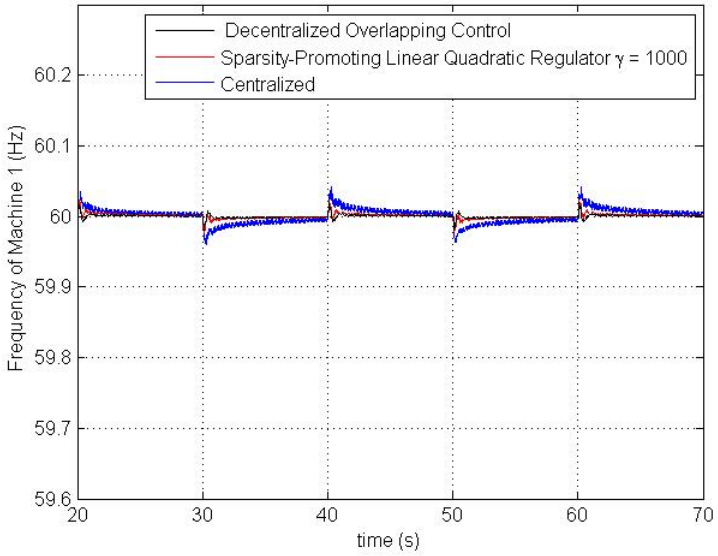

(a) Frequency Response of Machine 1

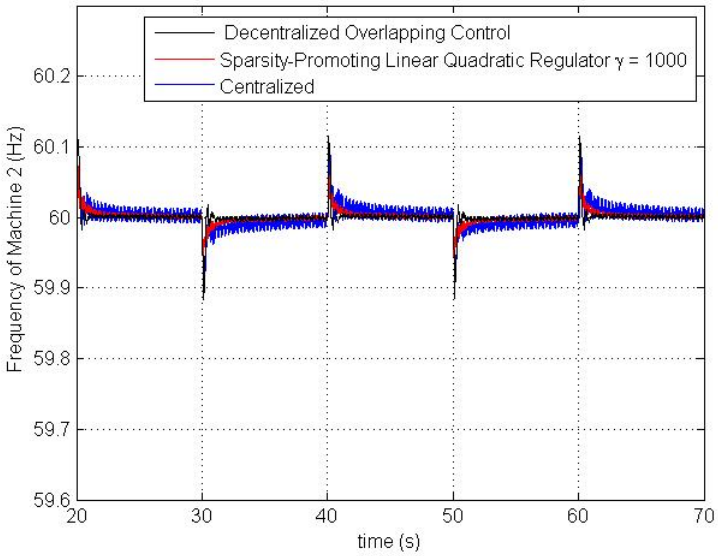

(b) Frequency Response of Machine 2

Figure 4.5: Subfigures (a) (b) and (c) display how the frequency of machines 1, 2 and 3 respectively change when the wind generation changes at $t = 30$ s, $t = 40$ s, $t = 50$ s and $t = 60$ s. Subfigure (d) displays tie-line flows across the two areas for the same disturbances. The plots show the response when the following controllers are employed: centralized controller, sparsity-promoting linear quadratic controller with $\gamma = 1000$, decentralized overlapping controller.

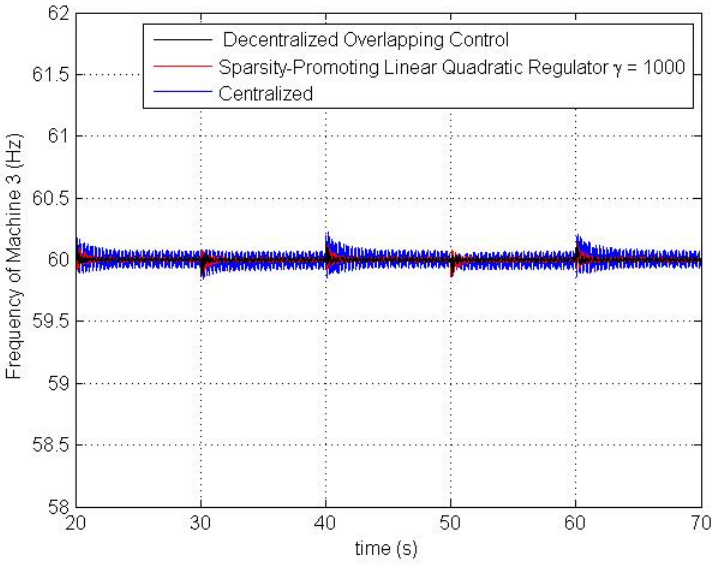

(c) Frequency Response of Machine 3

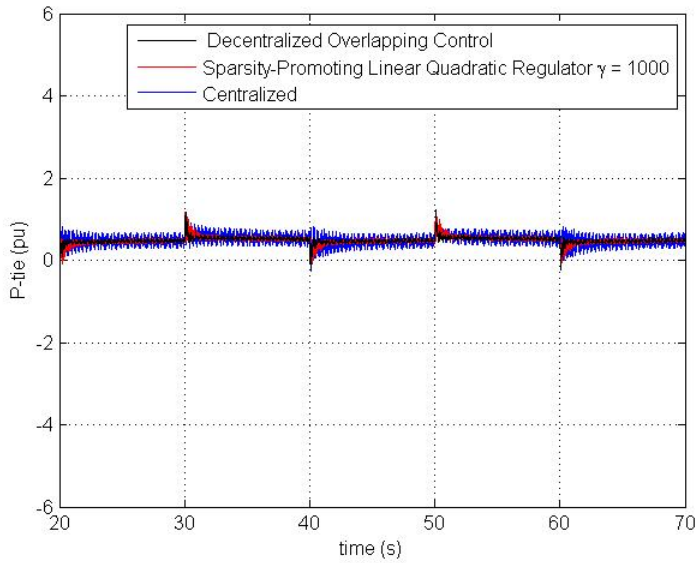

(d) Dynamic Response of tie-line flows across areas 1 and 2

Figure 4.5: Continued.

CHAPTER 5

CONCLUSION

In this thesis, we extended the traditional AGC systems to include wind-based generation and the system network, and proposed alternative decentralized controllers to stabilize the frequency and power interchange among different areas of an interconnected power system. The power injected by wind turbines was modeled as an uncertain disturbance to the system dynamics, and treated as negative load and subtracted from the actual system load. A power flow program is run at each AGC cycle to account for the network dynamics. We used a three-state nonlinear machine model that includes the mechanical equations and the governor dynamics to simulate the system. A partially decentralized state-feedback controller was designed using the theory of optimal control with an optimization algorithm (sparsity-promoting optimal control) to maximize the sparsity of the controller gain. Another decentralized controller was designed using the theory of overlapping control and the inclusion principle. Results show that overlapping control provides more decentralization with excellent performance compared to the sparsity-promoting optimal controller and to the centralized controller. Both controllers were able to track the desired frequency and power interchange with performance similar to the centralized controller regardless of load and wind disturbances.

APPENDIX A

ANGLE REFERENCES

Every rotational system must have a reference for angles. This reference can be arbitrarily chosen. As a result, the size of the multimachine model in Section 2.2 can be decreased by 1 state [20]. To show this, we define the angles relative to machine 1 as

$$\begin{aligned} \delta_i^{'} &:= \delta_i - \delta_1 \qquad i = 1, ..., m \\ \theta_i^{'} &:= \theta_i - \delta_1 \qquad i = 1, ..., m \end{aligned} \tag{A.1}$$

with the derivative of the dynamic states becoming

$$\begin{aligned} \frac{d\delta_1^{'}}{dt} &= 0 \\ \frac{d\delta_i^{'}}{dt} &= \omega_i - \omega_1 \qquad i = 2, ..., m \end{aligned} \tag{A.2}$$

where m is the number of machines and n is the number of buses. All angles in the algebraic equations in (2.7) can be written in terms of $\delta_i^{'}$ and $\theta_i^{'}$.

APPENDIX B

3-MACHINE 9-BUS 2-RENEWABLE RESOURCES CASE STUDY MATRICES

In this appendix we present the matrices obtained using the information in Section 4.1 following the model in (2.8).

$$A_1 = \begin{bmatrix} -0.1000 & 7.9736 & 0 & 0 & 0 & 0 & 0 & 0 \\ -0.2653 & -5.0000 & 0 & 0 & 0 & 0 & 0 & 0 \\ -1.0000 & 0 & 0 & 1.0000 & 0 & 0 & 0 & 0 \\ 0 & 0 & 0 & -0.2000 & 29.4524 & 0 & 0 & 0 \\ 0 & 0 & 0 & -0.2653 & -5.0000 & 0 & 0 & 0 \\ -1.0000 & 0 & 0 & 0 & 0 & 0 & 1.0000 & 0 \\ 0 & 0 & 0 & 0 & 0 & 0 & -0.3000 & 62.6231 \\ 0 & 0 & 0 & 0 & 0 & 0 & -0.2653 & -5.0000 \end{bmatrix}$$

$$A_2 = \begin{bmatrix} 0 & 0 & 0 & 0 & 0 & 0 & 0 & 0 & 0 & 0 & 0 & 0 \\ 0 & 0 & 0 & 0 & 438.5734 & -56.7378 & 0 & 0 & 0 & 0 & 0 & 0 \\ 0 & 0 & 0 & 0 & 0 & 0 & 0 & 0 & 0 & 0 & 0 & 0 \end{bmatrix}$$

$$A_3 = \begin{bmatrix} -3.9868 \\ 0 \\ 0 \\ -14.7262 \\ 0 \\ 0 \\ 62.6231 \\ 0 \end{bmatrix}$$

$$A_4 = \begin{bmatrix} 0.8639 & 0 & 0 & 0.8639 & 0 & 0 & -1.7278 & 0 \end{bmatrix}, A_5 = -0.0783$$

$$B_1 = \begin{bmatrix} 0 & 0 & 0 \\ 5 & 0 & 0 \\ 0 & 0 & 0 \\ 0 & 0 & 0 \\ 0 & 5 & 0 \\ 0 & 0 & 0 \\ 0 & 0 & 0 \\ 0 & 0 & 5 \end{bmatrix}, B_2 = 0.0058$$

$$C_1 = 1, C_2 = \begin{bmatrix} 0 & 0 & 0 & 0 & 0 & 0 & 0 & 0 \\ 0 & 0 & 0 & 0 & 0 & 0 & 0 & 0 \\ 0 & 0 & -0.5028 & 0 & 0 & 0 & 0 & 0 \\ 0 & 0 & -0.6751 & 0 & 0 & 0 & 0 & 0 \\ 0 & 0 & 0 & 0 & 0 & -7.0034 & 0 & 0 \\ 0 & 0 & 0 & 0 & 0 & -0.9060 & 0 & 0 \\ 0 & 0 & 0 & 0 & 0 & 0 & 0 & 0 \\ 0 & 0 & 0 & 0 & 0 & 0 & 0 & 0 \\ 0 & 0 & 0 & 0 & 0 & 0 & 0 & 0 \\ 0 & 0 & 0 & 0 & 0 & 0 & 0 & 0 \\ 0 & 0 & 0 & 0 & 0 & 0 & 0 & 0 \\ 0 & 0 & 0 & 0 & 0 & 0 & 0 & 0 \\ 0 & 0 & 0 & 0 & 0 & 0 & 0 & 0 \end{bmatrix}$$

$$C_3 = \begin{bmatrix} 20.4481 & 0.8260 & 0 & 0 & 0 & 0 & -5.9636 & 0.7850 & 0 & 0 & -13.6430 & 0.8174 \\ 0.8260 & -17.9880 & 0 & 0 & 0 & 0 & -0.7598 & -6.1614 & 0 & 0 & -0.8043 & -13.8648 \\ 0 & 0 & 16.0072 & 0 & 0 & 0 & 0 & 0 & -5.7444 & 0.4933 & -9.7599 & 0.1990 \\ 0 & 0 & 0.0041 & 0.0041 & 0 & 0 & 0 & 0 & -0.4834 & -5.8616 & -0.1958 & -9.9186 \\ 0 & 0 & 0 & -14.1999 & 29.0239 & 0.0008 & -11.3765 & -6.1614 & -11.5206 & -0.2693 & 0 & 0 \\ 0 & 0 & 0 & 0 & 0.0008 & -15.1583 & -0.4902 & -11.7538 & -0.4166 & -10.861 & 0 & 0 \\ -5.9636 & -0.7598 & 0 & 0 & -11.3765 & -0.4902 & 17.3401 & -1.2915 & 0 & 0 & 0 & 0 \\ -0.7598 & 5.9636 & 0 & 0 & -0.4902 & 11.3765 & 1.2500 & -16.8825 & 0 & 0 & 0 & 0 \\ 0 & 0 & -5.7444 & -0.4834 & -10.6440 & -0.4166 & 0 & 0 & 16.3884 & -0.9184 & 0 & 0 \\ 0 & 0 & -0.4834 & 5.7444 & -0.4166 & 10.6440 & 0 & 0 & 0.9000 & -16.110 & 0 & 0 \\ -13.6430 & -0.8043 & -9.7599 & -0.1958 & 0 & 0 & 0 & 0 & 0 & 0 & 23.4029 & -1.0163 \\ -0.8043 & 13.6430 & -0.1958 & 9.7599 & 0 & 0 & 0 & 0 & 0 & 0 & 1.0000 & -23.0737 \end{bmatrix}$$

$$D_1 = \begin{bmatrix} 0 & 0 & 0 \\ 0 & 0 & 0 \\ 0 & 0 & 0 \\ 0 & 0 & 0 \\ 0 & 0 & 0 \\ 0 & 0 & 0 \\ -1 & 0 & 0 \\ 0 & 0 & 0 \\ 0 & -1 & 0 \\ 0 & 0 & 0 \\ 0 & 0 & -1 \\ 0 & 0 & 0 \end{bmatrix}, D_2 = \begin{bmatrix} 0 & 0 & 0 \\ 0 & 0 & 0 \\ 0 & 0 & 0 \\ 0 & 0 & 0 \\ 0 & 0 & 0 \\ 0 & 0 & 0 \\ 0 & 0 & 0 \\ -1 & 0 & 0 \\ 0 & 0 & 0 \\ 0 & -1 & 0 \\ 0 & 0 & 0 \\ 0 & 0 & -1 \end{bmatrix}, D_3 = \begin{bmatrix} 0 & 0 \\ 0 & 0 \\ 0 & 0 \\ 0 & 0 \\ 0 & 0 \\ 0 & 0 \\ 0 & 0 \\ 1 & 0 \\ 0 & 0 \\ 0 & 1 \\ 0 & 0 \\ 0 & 0 \\ 0 & 0 \end{bmatrix}$$

Following the notation in (4.9) and (4.9), we have for A, B_1 and B_2

$$A_1 = \begin{bmatrix} -0.1000 & 7.9736 & 0.5614 & 0 & 0 & 5.4144 & 0 & 0 & -3.9868 & -0.0062 & -0.0057 \\ -0.2653 & -5.0000 & 0 & 0 & 0 & 0 & 0 & 0 & 0 & 0 & 0 \\ -1.0000 & 0 & 0 & 1.0000 & 0 & 0 & 0 & 0 & 0 & 0 & 0 \\ 0 & 0 & 2.5610 & -0.2000 & 29.4524 & 12.2928 & 0 & 0 & -14.7262 & -0.0121 & -0.0152 \\ 0 & 0 & 0 & -0.2653 & -5.0000 & 0 & 0 & 0 & 0 & 0 & 0 \\ -1.0000 & 0 & 0 & 0 & 0 & 0 & 1.0000 & 0 & 0 & 0 & 0 \\ 0 & 0 & 25.4215 & 0 & 0 & 417.1946 & -0.3000 & 62.6231 & 62.6231 & -0.3293 & -0.3524 \\ 0 & 0 & 0 & 0 & 0 & 0 & -0.2653 & -5.0000 & 0 & 0 & 0 \\ 0.8639 & 0 & 0.0009 & 0.8639 & 0 & 0.0080 & -1.7278 & 0 & 0 & 0 & 0 \\ 0 & 0 & 0 & 0 & 0 & 0 & 0 & 0 & 0 & -0.0783 & 0 \\ 0 & 0 & 0 & 0 & 0 & 0 & 0 & 0 & 0 & 0 & -0.0783 \end{bmatrix}$$

$$B_1 = \begin{bmatrix} 1.0741 & 0.9784 & 1.4662 & -0.0261 & 0.0400 & -0.0857 & 0 & 0 \\ 0 & 0 & 0 & 0 & 0 & 0 & 0 & 0 \\ 0 & 0 & 0 & 0 & 0 & 0 & 0 & 0 \\ 2.0807 & 2.6244 & 3.2039 & 0.2302 & -0.2943 & -0.2784 & 0 & 0 \\ 0 & 0 & 0 & 0 & 0 & 0 & 0 & 0 \\ 0 & 0 & 0 & 0 & 0 & 0 & 0 & 0 \\ 56.7832 & 60.7535 & 52.3715 & 0.5486 & -1.6303 & 1.5851 & 0 & 0 \\ 0 & 0 & 0 & 0 & 0 & 0 & 0 & 0 \\ 0.0016 & 0.0014 & 0.0021 & 0.0001 & 0.0000 & 0.0000 & 0 & 0 \\ 0 & 0 & 0 & 0 & 0 & 0 & 0.0058 & 0 \\ 0 & 0 & 0 & 0 & 0 & 0 & 0 & 0.0058 \end{bmatrix}$$

$$B_2 = \begin{bmatrix} 0 & 0 & 0 \\ 5 & 0 & 0 \\ 0 & 0 & 0 \\ 0 & 0 & 0 \\ \hline 0 & 5 & 0 \\ 0 & 0 & 0 \\ 0 & 0 & 0 \\ \hline 0 & 0 & 5 \\ 0 & 0 & 0 \\ 0 & 0 & 0 \\ \hline 0 & 0 & 0 \end{bmatrix}$$

APPENDIX C

STANDARD LINEAR QUADRATIC REGULATOR PROBLEM

Let a dynamical system be described by

$$\dot{x} = Ax + Bu \tag{C.1}$$

where $x(0) = x_0$ is arbitrary and (A,B) is stabilizable. Find the optimal control law $u(t)$ that drives the states to zero and minimizes the cost

$$J = \int_0^\infty (x(t)^T Q x(t) + u(t)^T R u(t)) dt \tag{C.2}$$

where $Q \geq 0$ and $R > 0$. The optimal solution is $u(t) = -Kx$ where

$$K = R^{-1} B^T X \tag{C.3}$$

and $X = X^T \geq 0$ is the unique solution of the algebraic Riccati equation [27]

$$A^T X + XA - XBR^{-1}B^T X + Q = 0 \tag{C.4}$$

REFERENCES

[1] U.S. Department of Energy, "The smart grid: an introduction," [Online]. Available: http://www.oe.energy.gov/smartgrid.htm [Oct. 01, 2015]

[2] T. Ackermann, *Wind Power in Power Systems*. Chichester, West Sussex, England: John Wiley and Sons, Ltd., 2005.

[3] BTM Consult APS (2013). "International Wind Energy Development-Forecast 2013-2017". [Online]. Available: http://www.navigantresearch.com/wp-content/uploads/2013/03/WWMU-13-Executive-Summary.pdf [Oct. 01, 2015]

[4] E. DeMeo, G. Jordan, C. Kalich, J. King, M. Milligan, C. Murley, B. Oakleaf, and M. Schuerger, "Accommodating wind's natural behavior," *IEEE Power and Energy Magazine* vol. 5, no. 6, pp. 59-67, Nov.-Dec. 2007.

[5] H. Bevrani. *Robust Power System Frequency Control*. New York: Springer, 2009.

[6] J. Morren, J. Pierik and S. W. de Haan, "Inertial response of variable speed wind turbines, " *Electric Power Systems Research*, vol. 76, no. 11, pp. 980 - 987, July 2006.

[7] European Wind Integration Study (EWIS) (2007). "Towards a Successful Integration of Wind Power into European Electricity Grids." [Online]. Available: http://www.wind-integration.eu/downloads/library/EWIS-phase-I-final-report.pdf [Oct. 01, 2015]

[8] H. Illian, "Frequency control performance measurement and requirements," Lawrence Berkeley National Laboratory, Tech. Rep. LBNL-4145E, December 2010.

[9] C. Martinez, S. Xue, and M. Martinez, "Review of the recent frequency performance of the Eastern, Western and ERCOT interconnections," Lawrence Berkeley National Laboratory, Tech. Rep. LBNL-4144E, December 2010.

[10] C. E. Fosha, O. I. Elgerd, "The megawatt-frequency control problem: A new spproach via optimal control theory," *Proceedings, Power Industry Computer Applications Conference*, 1969.

[11] V.R. Moorthi, R.P. Aggarwal, "Suboptimal and near-optimal control of a load-frequency-control system," *Proceedings of the Institution of Electrical Engineers,* vol. 119, no. 11, pp. 1653-1660, November 1972.

[12] S.S. Choi, H.K. Sim, K.S. Tan, "Load frequency control via constant limited-state feedback," *Electric Power Systems Research*, vol. 4, no. 4, October 1981, pp. 265-269.

[13] J. Undrill, "Power and frequency control as it relates to wind-powered generation," Lawrence Berkeley National Laboratory, Tech. Rep. LBNL-4143E, December 2010.

[14] A. D. Dominguez-Garcia, "Models for impact assessment of wind-based power generation on frequency control," in *Control and Optimization Methods for Electric Smart Grids*, vol. 3, A. Chakrabortty, and M. Ilić (Eds.), Springer-Verlag, Berlin, 2012.

[15] F. Lin, M. Fardad, and M. R. Jovanovic, "Design of optimal sparse feedback gains via the alternating direction method of multipliers," *IEEE Trans. Automat. Control*, vol. 58, no. 9, pp. 2426-2431, 2011.

[16] F. Dörfler, M. R. Jovanović, M. Chertkov and F. Bullo, "Sparsity-promoting optimal wide-area control of power networks," *IEEE Transactions of Power Systems*, vol. 29, no. 5, pp. 2281-2291, 2014.

[17] D. D. Ŝiljak, *Large-Scale Dynamic Systems: Stability and Structure*. New York, NY: North-Holland, 1978.

[18] M. Ikeda, D. D. Ŝiljak, "Overlapping decentralized control with input, state, and output inclusion," *Control-Theory and Advanced Technology*, 2, pp. 155-172, 1986.

[19] D. D. Ŝiljak, *Decentralized Control of Complex Systems*. Boston, MA: Academic Press, 1991

[20] P. Sauer and A. Pai, *Power System Dynamics and Stability*. Upper Saddle River, NJ: Prentice Hall, 1998.

[21] H. A. Pulgar-Painemal, "Reduced-order model of type-c wind turbine generators," *Electric Power Systems Research*, vol. 81, no. 4, pp. 840 - 845, 2011.

[22] H. A. Pulgar-Painemal, "Wind farm model for power system stability analysis," Ph.D. dissertation, University of Illinois at Urbana-Champaign, 2010.

[23] A. J. Wood and B. F. Wollenberg, *Power Generation, Operation, and Control*. Second edition, John Wiley & Sons, Singapore, 1996.

[24] M. Ikeda, D. D. Ŝiljak, D. E. White, "An inclusion principle for dynamic systems," *IEEE Transactions on Automatic Control*, 29, 244-249, 1986.

[25] D. Stipanović, G. Inalhan, R. Teo and C. Tomlin, "Decentralized overlapping control of a formation of unmanned aerial vehicles," *Automatica*, vol. 40, no.8, pp. 1285-1296, August, 2004.

[26] F. Lin, M. Fardad, and M. R. Jovanovic, "Sparsity-promoting linear quadratic regulator," [Online]. Available: http://www.ece.umn.edu/users/mihailo/software/lqrsp/index.html, [Oct. 01, 2015]

[27] S. Skogestad and I. Postlethwaite, *Multivariable Feedback Control: Analysis and Design*. John Wiley & Sons, 2005.